metals

MDPI

Article

Comparison of Hydrostatic Extrusion between Pressure-Load and Displacement-Load Models

Shengqiang Du [1], Xiang Zan [1,2,*], Ping Li [1], Laima Luo [1,2], Xiaoyong Zhu [2] and Yucheng Wu [1,2,*]

1 School of Materials Science and Engineering, Hefei University of Technology, Hefei 230009, China; 15255150652@163.com (S.D.); li_ping@hfut.edu.cn (P.L.); luolaima@126.com (L.L.)

2 National–Local Joint Engineering Research Centre of Nonferrous Metals and Processing Technology, Hefei 230009, China; zhuxiaoyong@hfut.edu.cn

* Correspondence: zanx@hfut.edu.cn (X.Z.); ycwu@hfut.edu.cn (Y.W.); Tel.: +86-551-6290-1367 (X.Z.); +86-551-6290-1012 (Y.W.)

Academic Editors: Myoung-Gyu Lee and Yannis P. Korkolis
Received: 25 October 2016; Accepted: 27 February 2017; Published: 1 March 2017

Abstract: Two finite element analysis (FEA) models simulating hydrostatic extrusion (HE) are designed, one for the case under pressure load and another for the case under displacement load. Comparison is made of the equivalent stress distribution, stress state ratio distribution and extrusion pressure between the two models, which work at the same extrusion ratio (R) and the same die angle (2α). A uniform Von-Mises equivalent stress gradient distribution and stress state ratio gradient distribution are observed in the pressure-load model. A linear relationship is found between the extrusion pressure (P) and the logarithm of the extrusion ratio ($\ln R$), and a parabolic relationship between P and 2α, in both models. The P-value under pressure load is smaller than that under displacement load, though at the same R and α, and the difference between the two pressures becomes larger as R and α grow.

Keywords: hydrostatic extrusion; FEA; pressure load; die angle; extrusion ratio

1. Introduction

Hydrostatic extrusion (HE) is a unique forming method that was presented by Robertson in 1893 [1]. During the process, the material is surrounded by a high-pressure medium, which forms hydrostatic pressure conditions that improve the material's formability; thereby, larger amounts of deformation can be achieved as compared to the conventional extrusion process. The medium also ensures good lubricant conditions, and even generates dynamic lubrication between the die and the billet [2], and hence great surface quality. HE as a special severe plastic deformation (SPD) method has great advantages for large deformation processes and the forming processes of difficult-to-form materials.

By using the HE process, Ozaltin et al. [3] improved the strength of Ti-45Nb by 45% and also attained good plasticity by refining the grain. Also, by HE, Yu et al. [4] realized the deformation of AZ31 at 200–300 °C, at a maximum R of 31.5. Xue et al. [5] improved the properties of Zr-based metallic glass/porous tungsten phase composite; the breaking strength reaching 2112 MPa and the fracture strain reaching 53%. Kaszuwara et al. [6] densified Nd-Fe-B powder to the theoretical maximum density by HE. Kováč et al. [7] prepared MgB_2 wires by internal magnesium diffusion and HE. Skiba et al. [8] deformed GJL250 grey cast iron and GJS500 nodular cast iron by improved HE equipment with back pressure. Hydrostatic extrusion is widely used in the preparation of materials which are hard to deform. Finite element analysis (FEA) has also been used for investigations of the HE processes. Zhang et al. [9] simulated the HE process with tungsten alloy; the displacement load on the upper surface and a rigid boundary on the lateral surface of the billet were used instead of the pressure load of the pressure medium. Li et al. [10] simulated the HE process of W-40 wt. % Cu at

650–800 °C with simplified boundary conditions and calculated the linear relationship between the extrusion pressure and temperature, and proved the simulation results with experiments. Replacing the pressure of a pressure medium with a displacement load, accompanied by near-zero friction between the billet surface and the virtual rigid container, it is easy to model the HE process and improve the convergence rate effectively. However, without hydrostatic pressure, the simulation results reduce the accuracy and differ from real hydrostatic extrusion. In Li's work [10], a large gradient of equivalent stress distribution at the un-deformed region surrounded by the pressure medium was found, which was different from the real HE process where that region was in a hydrostatic state and the equivalent stress should be almost near zero. Thus, using the simplified displacement-load mode may introduce inaccuracy into the simulation results. Manafi and Saeidi [11] simulated 93 tungsten alloy by HE with a pressure boundary condition and found the optimized die angle. Peng et al. [12], by calculating the stress distribution in Nb/Cu composited by HE, investigated its interface bonding status. Manifi et al. [13] improved conventional backward extrusion by employing HE principles to reduce the extrusion load; the maximum load was reduced by 80% compared to the conventional back extrusion process. Kopp and Barton [14] improved the model of HE and analyzed the differences between experimentation and simulation.

The comparisons between the simulation and experiment were discussed in [10–14], but the comparison between the different simulation models has not been discussed in detail yet. In the present study, the pressure-load mode and displacement-load mode are used to simulate the HE process. In addition, the main work of this paper is comparing the deviation of the calculated results of the two modes under the same conditions and finding out the influence of the pressure. The judgments of the comparison are made through the theories of HE.

2. FEM Methods and Materials

The biggest difference between hydrostatic extrusion and conventional extrusion lies in the way of transferring loads from the punch to the billet. In HE process, the billet is tapered to match the die geometry, the gap between the billet and the container is filled with pressure medium, which surrounds the billet and conveys the extrusion force of the moving punch onto it, and the pressure medium is forced by its inherent pressure into the gap between the die and the billet, generating excellent lubrication on the contact surface (Figure 1a). In the present study, castor oil is used as the liquid pressure medium. The billet is tapered to match the die geometry before the extrusion in order to ensure the pressure medium staying in the container. In the real experiment, the gaps between the punch, container and the die were sealed by rubber and pure copper seal rings to ensure the system is under good sealing state. While, in the conventional extrusion, the billet is pressed by the punch directly (Figure 1b) and so deformed.

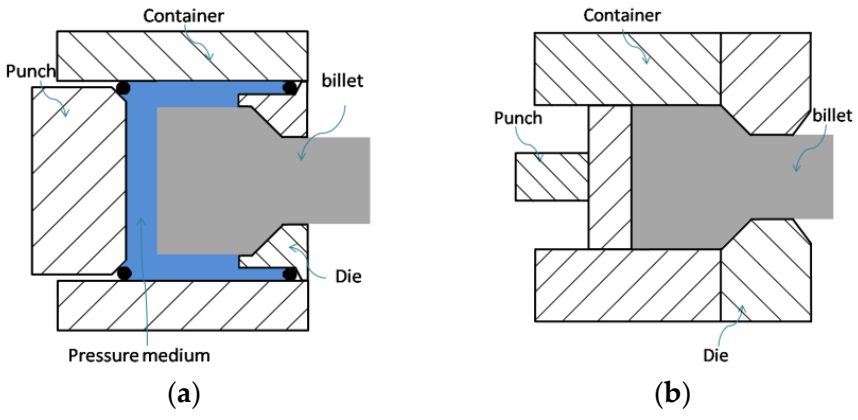

Figure 1. Principle of (**a**) hydrostatic extrusion and (**b**) conventional extrusion.

To simulate the HE process accurately, it has to take the fluid-structure interaction mode, which, however, is too complicated for large-scale calculation. So, the model developed in the present study is a partly simplified one, which improves the calculation efficiency and ensures the calculation precision. The numerical software ANSYS (V15.0, ANSYS Inc., Canonsburg, PA, USA) was used for the simulation. In the model, the pressure medium is replaced by uniform pressure loads, the die is partly replaced by rigid lines, and no friction is set between the billet and the fluid while friction between the billet and the die is in agreement with Coulomb's friction law. The model could be further simplified to 2-D because of the axial symmetry of both billet and die as columns. An eight-node plane element (PLANE 183) is used.

The pressure load mode is the mode replacing the pressure medium as a boundary condition of the billet, modeling only its pressure properties. The pressure is set to increase linearly with the time, replacing the effect of the punch pushing the pressure medium. So, in this model, the punch is not needed because the billet is deformed by the increased pressure. In the pressure load model, the central axis of the billet is the symmetrical axis of both billet and die, and the pressure load only exists over the un-deformed outer surface of the billet. The fillet at upper right of the billet is built to verify the uniform distribution of the pressure load. The coefficient of friction between the billet and the die is set as 0.05 (Figure 2a). A displacement load model which is commonly used is also established, for the sake of comparison (Figure 2b). In the displacement load mode, the displacement load with even speed is directly applied on the upper surface of the billet. The lateral surface of the billet is constrained by displacement constraint to ensure the materials cannot flow along the positive direction of the radius. Thus, the extrusion force can be calculated by the reaction force. Rigid lines are placed outside the un-deformed region instead of the displacement constraint and the coefficient of friction over this region is set as 0 which replaces the zero friction between billet and pressure medium. So, the displacement load mode is essentially a conventional extrusion mode without friction between the billet and the die. The material used to be deformed in both models is AA2024, which is a typical ideal elastoplastic material, whose specific parameters are given in Table 1. The two models are simulated at room temperature (298 K), and the parameters used for the simulations presented in this paper are given in Table 2.

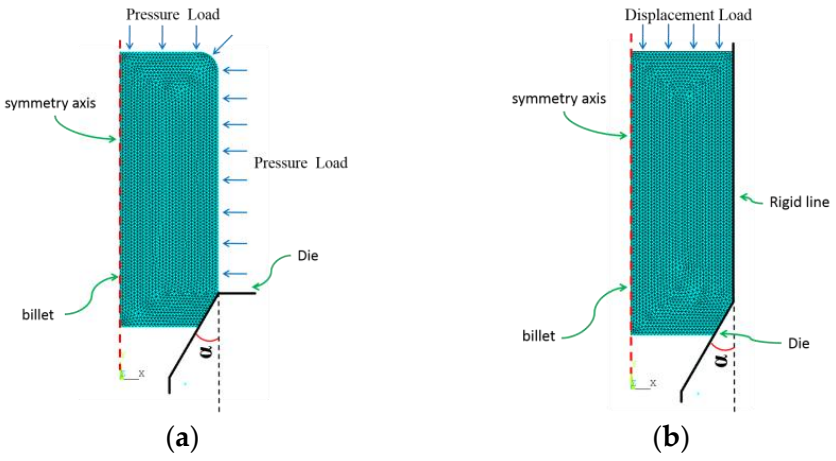

Figure 2. Models of (**a**) pressure load and (**b**) displacement load.

Table 1. Material properties of AA2024.

Material	Density	Poisson Ratio	Elastic Modulus	Yield Stress
AA2024	2.79 g/cm^3	0.3	71.7 GPa	340 MPa

Table 2. Simulation parameters of pressure load mode and displacement load mode.

Load Mode	Extrusion Ratio	Die Angle (2α)	Initial Height	Initial Diameter
Pressure load	2.25, 2.78, 4.00, 6.25	25°, 30°, 35°, 40°, 60°, 90°, 120°	80 mm	30 mm
Displacement load				

3. Results and Discussion

As shown in Figure 3, fluid pressure changed with time as the set pressure was distributed uniformly over the outer surface of the un-deformed region of the billet and decreases gradually and finally disappeared near the entrance of the die. The distributions of the pressure at different stages all proved that the hydrostatic pressure property was perfectly represented. The pressure changed linearly with time and reached a certain amount when the billet was deformed. The distribution of the fluid pressure, again as shown in Figure 3, proved that the pressure load model fits the real HE process well.

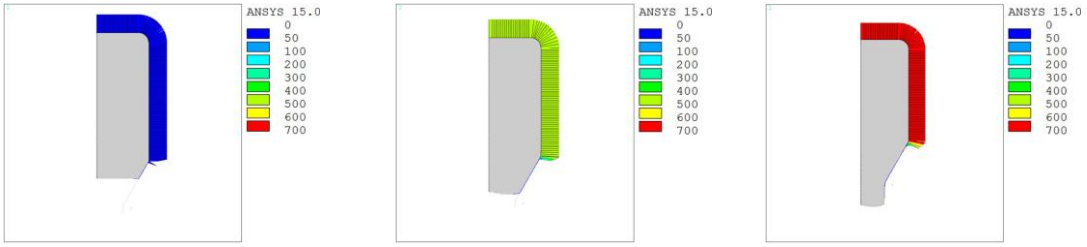

Figure 3. Fluid pressure distribution at (**a**) initial stage; (**b**) pressure-up stage and (**c**) stable stage.

3.1. Comparison of Distribution of Stress and Strain Field

The distribution information, including the equivalent strain, equivalent stress, etc., as calculated, was compared under the same scale bar, between the two models, thus making the difference much more obvious. The comparison was conducted at R = 4.00 and 2α = 60°.

The Von-Mises equivalent strain distributions of the two models (Figure 4) were found to be basically the same, proving that the comparison was conducted as the two billets were experiencing the same degree of deformation.

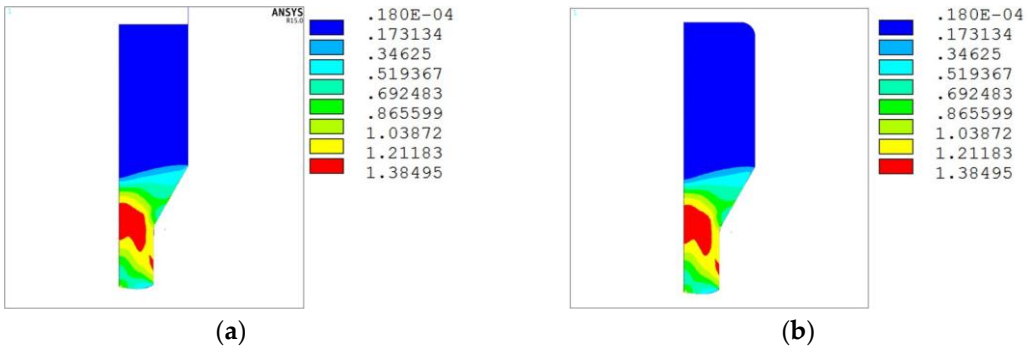

Figure 4. Von-Mises equivalent strain distribution of (**a**) displacement-load model and (**b**) pressure-load model.

The axial stress distributions (Figure 5) indicate that, on the surface of the billet under pressure load, the area of the compressed stress–concentrated region in the inlet region was larger and that of the tensile stress–concentrated region was smaller in the outlet region than those in the case of

displacement load. These differences can affect the material's formability. So in the pressure-load model, there was less of a tendency to generate cracks on the surface of the billet when the material went through the inlet and outlet regions, and hence there was good surface quality, which is an important characteristic of HE.

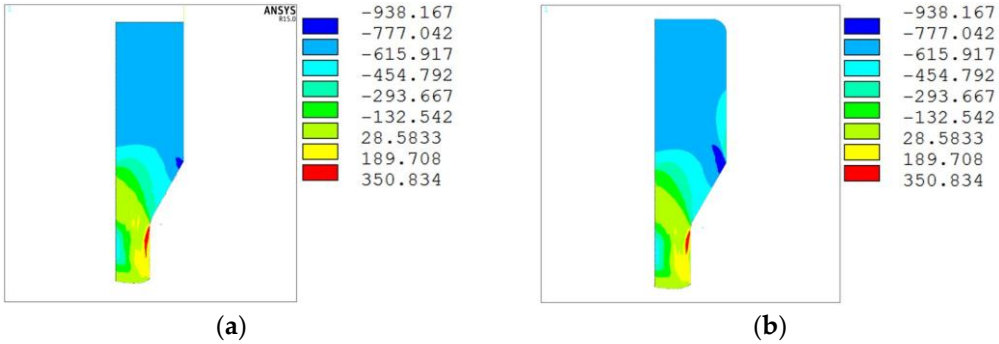

Figure 5. Axial distribution of (**a**) displacement-load model and (**b**) pressure-load model.

The Von-Mises equivalent stress distributions of the two models were obviously different, just as shown in Figure 6. It was found that, under displacement load, the material was pressed by unequal σ_1, σ_2, σ_3, generating an exorbitant Von-Mises stress in the un-deformed region and a tiny Von-Mises stress in a small region only in the core of the billet at the inlet of the die, which is totally different from the situation of the real HE process (Figure 6a). The Von-Mises equivalent stress was extremely small in the un-deformed region under pressure load, because the billet was surrounded by hydrostatic pressure, which made the primary stress (σ_1, σ_2, σ_3) nearly equal. The value of the equivalent stress gradually reached the yield value as the deformation went on, and so there exists a gradient distribution of the equivalent stress in the inlet region, where the deformed and un-deformed regions are clearly demarcated (Figure 6b). In Reference [10], the stress distribution with a large value was found in the un-deformed region, proving the mode in that work was similar to the displacement load. In addition, this equivalent stress difference indicates that the pressure-load model is more suitable for HE analysis.

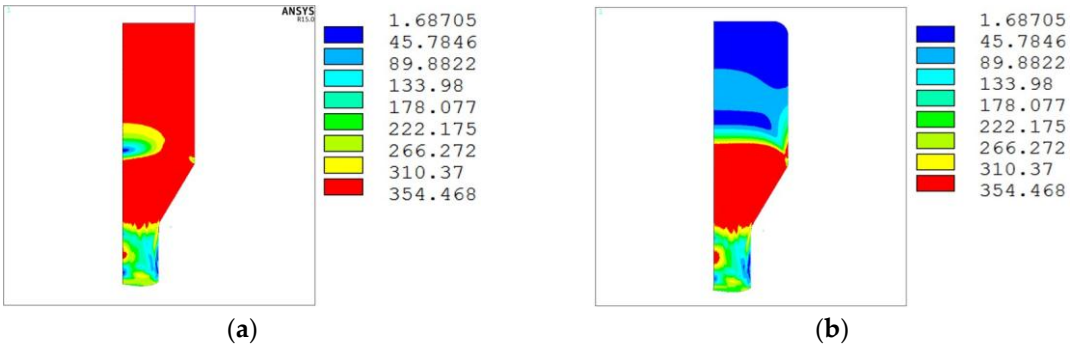

Figure 6. Von-Mises equivalent stress distribution of (**a**) displacement load and (**b**) pressure load.

The equivalent strain and stress distributions of the pressure-load model proved the un-deformed region was under hydrostatic pressure, ensuring no deformation was happening. Some experiments [15,16] were conducted to verify the materials' deformation behavior through HE. The billet was cut through the center along the extrusion axis and a grid was printed on the cut surface. Finally, the two parts were put together and extruded. After extrusion, no deformation was found at the grid in the part surrounded by the pressure medium, the un-deformed region. The experiments fit the simulation results well.

The deformed region can be distinguished by the stress state ratio distribution. The boundary between the deformed and un-deformed regions under displacement load was not stable, lower in the core and higher near the surface (Figure 7a). In the case of pressure load, the boundary was parallel to the top surface, shaped like the Von-Mises equivalent stress distribution, thus proving that the material flowed uniformly under the hydrostatic pressure (Figure 7b). The die limited the material's movement during the deformation, making the material flow more easily in the core but less near the surface. The hydrostatic pressure can effectively improve the material's flow, for the material flowed uniformly even where the die exerts its limitation. However, the displacement load cannot benefit the material's flow, hence the uneven flow and the deformation near the surface lagging behind that in the core.

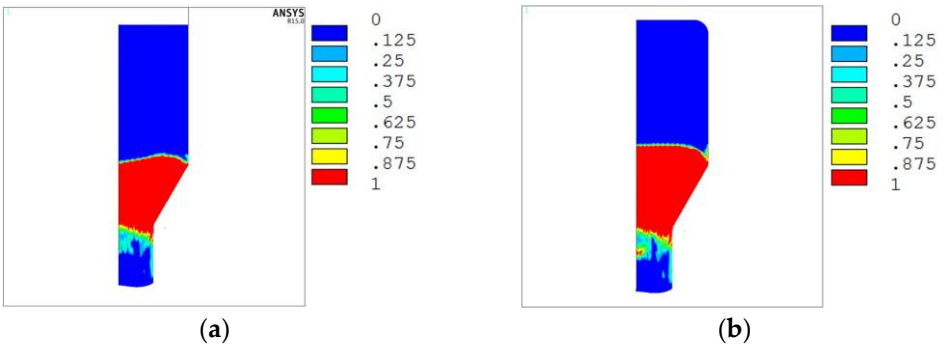

Figure 7. Stress state ratio distribution of (**a**) displacement load (**b**) and pressure load.

As can be seen in the contact pressure distribution, the material's flow near the surface differed between the two models. The contact pressure in the inlet region was higher under displacement load (Figure 8a) because uneven material flow results in more redundant work, so the load to achieve the same deformation is higher, hence the higher contact pressure. A lower contact pressure can be found under pressure load because the material deforms uniformly in this region and so lower redundant work is needed, hence the lower contact pressure (Figure 8b). Hydrostatic pressure can make the material flow uniformly, as was obviously shown in the pressure-load model.

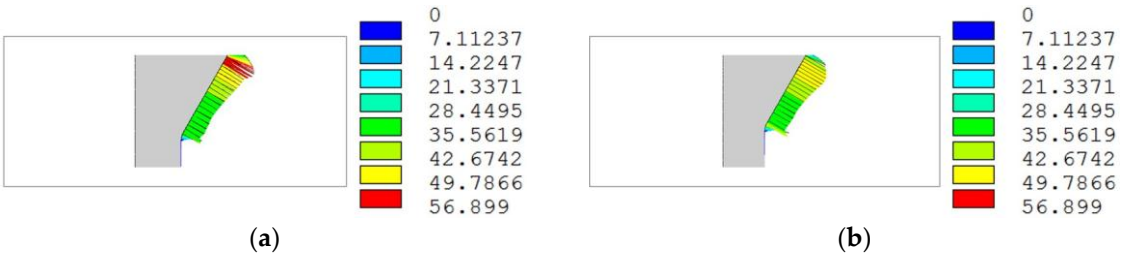

Figure 8. Contact pressure distribution of (**a**) displacement load and (**b**) pressure load.

3.2. Comparison of Extrusion Pressure

By analyzing the difference in HE, a further comparison was made between the two models. R is the deformation ratio, written as $R = D^2/d^2$. In the pressure-load model, the pressure increased linearly with the time; meanwhile, the billet was deformed. The pressure corresponding to the position when the bottom of the billet is pressed out of the die is the extrusion pressure (P), and this is the minimum pressure to complete the extrusion process. In the displacement-load model, the position with same deformation ratio can be found, and the extrusion pressure was calculated by the reaction force and the area of the contact surface. A linear relationship exists between P and ln$R$ in both models; for instance, at $\alpha = 45°$, $P = 424\ln R + 197$ for displacement load and $P = 347\ln R + 160$ for pressure load, respectively (Figure 9a). The pressure gap between the two load models can be found under the same working

conditions. The *P*-value is higher in the displacement-load model, because the material flows less uniformly, so that a higher *P* is required to overcome the redundant work. But under a pressure load, the *P*-value is lower because the hydrostatic pressure load can maintain uniform deformation during the process. The gap becomes larger as the *R* value increases, because the deformation uniformity decreases as the deformation ratio grows. However, the gap grows only a bit, indicating that the deformation ratio is not the main cause for the redundant work.

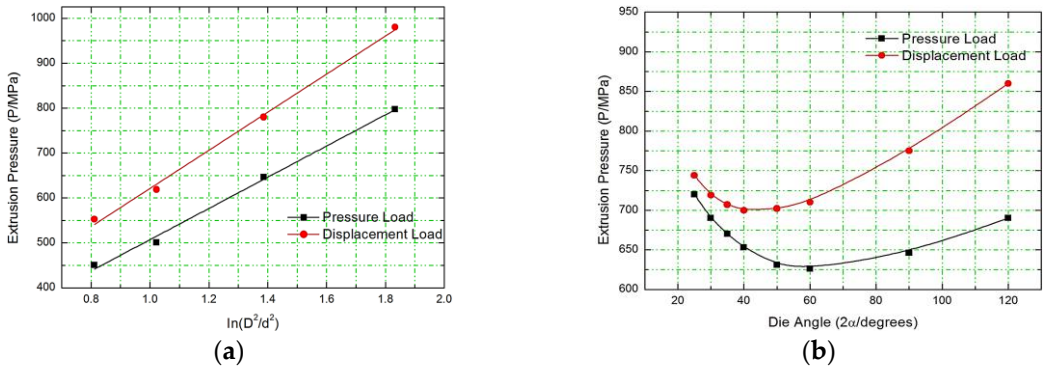

Figure 9. Relationship between (**a**) *P* and ln*R*; (**b**) *P* and 2*α*.

In both models, there exists a parabolic relationship between *P* and 2*α* (Figure 9b). Extrusion pressure first declined and then increase when 2*α* increased from 30° to 120°. The optimized die angle (2*α*), corresponding to the smallest *P*-value, was 40° and 60° in the displacement-load and the pressure-load model, respectively. The size of the optimized die angle depends on the redundant work and friction work during the deformation. The redundant work, resistant to non-uniform deformation, increased rapidly when the die angle grew. Meanwhile, the friction work also changed because both the contact pressure and contact area changed. As the die angle grew, the contact pressure increased whereas the contact area decreased, and the friction work first declined and then increased. The redundant work increase was lower than the friction work decrease at first, so the *P*-value declined, but as the die angle grew, the redundant work increase gradually grew faster than the friction work decrease, leading to the rise of the *P*-value. The pressure gap between the two models became larger rapidly as 2*α* grew, indicating that the redundant work increased faster in the displacement-load model. The gap grew rapidly with the die angle, indicating the angle was the main cause for the redundant work.

The relationship between *P* and 2*α* can be well explained by the stress state ratio distribution (Figure 10). As the die angle grew from 30° to 120°, the deformation region boundary in the displacement-load model increased more rapidly than in the pressure-load model and the shape of the boundary changed more drastically at the same time. The irregularity of the boundary indicated a non-uniform deformation, so more redundant work was generated, which in turn resulted in greater extrusion pressure to achieve the same deformation. So the extrusion pressure was lower in the pressure load model at the same die angle where the boundary was more stable. In addition, because of the hydrostatic pressure, little redundant work was generated in the pressure-load model, so the extrusion pressure value fluctuated in a small range at different die angles.

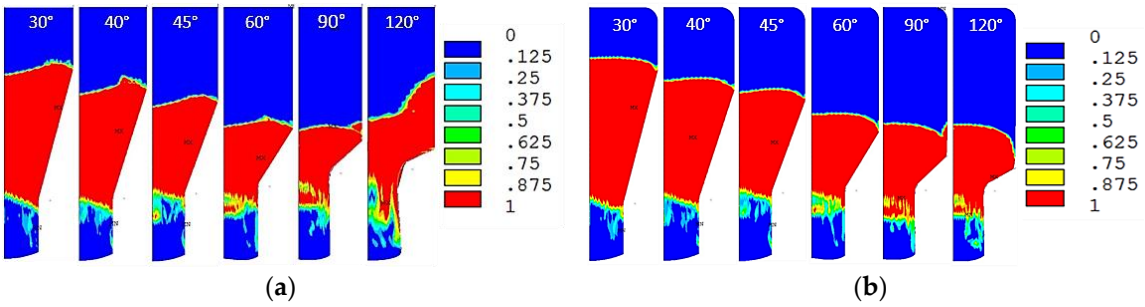

Figure 10. Stress state ratio distribution of (**a**) displacement-load model and (**b**) pressure-load model at $2\alpha = 30^\circ$, 40°, 45°, 60°, 90° and 120°.

4. Conclusions

Through numerical simulation, two models, the displacement-load model and pressure-load model, are designed and compared. Both models can simulate the hydrostatic extrusion process to a certain extent, gaining similar results of the strain calculation. Under the pressure load, the value of the Von-Mises equivalent stress in the un-deformed region is very small, which proves that this region is under uniform hydrostatic pressure. The deformation boundary in the stress state ratio distribution is almost horizontal, which proves that the material is pressed by hydrostatic pressure. However, in the displacement-load model, the Von-Mises stress value is large, and the deformation boundary is irregular, proving that, with no hydrostatic pressure, the deformation is non-uniform. The relationship between P and R was found as $P = 347\ln R + 160$ or $P = 424\ln R + 197$ in the pressure-load and displacement-load model. In addition, the optimized die angle was 60° or 40°, respectively. It can be proved that in the displacement-load model, the non-uniform material flow generates more redundant work, resulting in a higher extrusion pressure to achieve the same deformation. With the increase of the die angle, the abnormal growth of the extrusion pressure under displacement load indicates that the redundant work increases rapidly, which will lead to the deviation of the calculation results from the actual HE process. By comparing the data above, it is found that the numerical model with pressure load can simulate the hydrostatic extrusion process more accurately.

Acknowledgments: The authors would like to acknowledge the financial support from the National Magnetic Confinement Fusion Program with Grant No. 2014GB121001, the National Natural Science Foundation of China No. 51675154, and the research support from the Laboratory of Nonferrous Metal Material and Processing Engineering of Anhui Province.

Author Contributions: Shengqiang Du, Xiang Zan and Ping Li designed the simulation models; Shengqiang Du performed the simulation; Xiang Zan, Laima Luo and Xiaoyong Zhu contributed to analyze the simulation results; Yucheng Wu provided support and contributed to the discussions; Shengqiang Du wrote the paper.

Conflicts of Interest: The authors declare no conflict of interest.

References

1. Robertson, J. Method of and Apparatus for Forming Metal Articles. British Patent No. 19 356, 14 October 1894.
2. Wilson, W.R.D.; Walowit, J.A. An isothermal hydrodynamic lubrication theory for hydrostatic extrusion and drawing processes with conical dies. *J. Lubr. Technol.* **1971**, *93*, 69–74. [CrossRef]
3. Ozaltin, K.; Chrominski, W.; Kulczyk, M.; Panigrahi, A.; Horky, J.; Zehetbauer, M.; Lewandowska, M. Enhancement of mechanical properties of biocompatible Ti–45Nb alloy by hydrostatic extrusion. *J. Mater. Sci.* **2014**, *49*, 6930–6936. [CrossRef]
4. Yu, Y.; Zhang, W.C.; Duan, X.R. Study on microstructure and properties of thin tube of AZ31 magnesium alloy by extrusion technology. *Powder Metall. Technol.* **2013**, *31*, 201–206. [CrossRef]
5. Xue, Y.F.; Cai, H.N.; Wang, L.; Wang, F.C.; Zhang, H.F. Strength-improved Zr-based metallic glass/porous tungsten phase composite by hydrostatic extrusion. *Appl. Phys. Lett.* **2007**, *90*, 081901. [CrossRef]

6. Kaszuwara, W.; Kulczyk, M.; Leonowicz, M.K.; Gizynski, T.; Michalski, B. Densification of Nd-Fe-B powders by hydrostatic extrusion. *IEEE Trans. Magn.* **2014**, *50*, 1–5. [CrossRef]
7. Kováč, P.; Hušek, I.; Melišek, T.; Kopera, L.; Kováč, J. Critical currents, I_c-anisotropy and stress tolerance of MgB_2 wires made by internal magnesium diffusion. *Sci. Technol.* **2014**, *27*, 88–93. [CrossRef]
8. Skiba, J.; Pachla, W.; Mazur, A.; Przybysz, S.; Kulczyk, M.; Przybysz, M.; Wróblewska, M. Press for hydrostatic extrusion with back-pressure and the properties of thus extruded materials. *J. Mater. Process. Technol.* **2014**, *214*, 67–74. [CrossRef]
9. Zhang, Z.H.; Wang, F.C.; Sun, M.Y.; Yang, R.; Li, S.K. Finite element analysis and experimental investigation of the hydrostatic extrusion process of deforming two-layer Cu/Al composite. *J. Beijing Inst. Technol.* **2013**, *22*, 544–549. (In Chinese).
10. Li, D.R.; Liu, Z.Y.; Yu, Y.; Wang, E.D. Numerical simulation of hot hydrostatic extrusion of W-40 wt. % Cu. *Mater. Sci. Eng. A* **2009**, *499*, 118–122. [CrossRef]
11. Manafi, B.; Saeidi, M. Deformation behavior of 93 Tungsten alloy under hydrostatic extrusion. *Elixir Mech. Eng.* **2014**, *76*, 28487–28492.
12. Peng, X.; Sumption, M.D.; Collings, E.W. Finite element modeling of hydrostatic extrusion for mono-core superconductor billets. *IEEE Trans. Appl. Supercond.* **2003**, *13*, 3434–3437. [CrossRef]
13. Manafi, B.; Shatermashhadi, V.; Abrinia, K.; Faraji, G.; Sanei, M. Development of a novel bulk plastic deformation method: Hydrostatic backward extrusion. *Int. J. Adv. Manuf. Technol.* **2016**, *82*, 1823–1830. [CrossRef]
14. Kopp, R.; Barton, G. Finite element modeling of hydrostatic extrusion of magnesium. *J. Technol. Plast Technol.* **2003**, *28*, 1–12.
15. Barton, G. Finite-Elemente Modellierung des Hydrostatischen Strangpressens von Magnesiumlegierungen. Ph.D. Thesis, Rheinisch-Westfaelische Technische Hochschule Aachen, Aachen, Germany, January 2009. Available online: http://publications.rwth-aachen.de/record/51193/files/Barton_Gabriel.pdf (accessed on 1 March 2017).
16. Kulczyk, M.; Przybysz, S.; Skiba, J.; Pachla, W. Severe plastic deformation induced in Al, Al-Si, Ag and Cu by hydrostatic extrusion. *Arch. Metall. Mater.* **2014**, *59*, 59–64. [CrossRef]